Rev.Adv.Mater.Sci. 15(2007) 111-117

HARDNESS AND RESIDUAL STRESSES IN TiN-Ni NANOCOMPOSITE COATINGS DEPOSITED BY REACTIVE DUAL ION BEAM SPUTTERING

Alireza Akbari[1,2], Jean Paul Riviere[1], Claude Templier[1], Eric Le Bourhis[1] and Grégory Abadias[1]

[1]Laboratoire de Métallurgie Physique, UMR 6630 CNRS- Université de Poitiers, Bd M. et P. Curie, BP30179, 86962 Chasseneuil Futuroscope, France

[2]Department of Materials Engineering, Sahand University of Technology, PO Box 51335-1996, Tabriz, Iran

Received: January 22, 2007

Abstract. Nanocomposite coatings of nc-TiN/a-Ni were deposited using an ultrahigh vacuum dual ion beam sputtering technique, which consist in sputtering a composite Ti-Ni target with 1.2 keV Ar^+ ions while the growing film is bombarded with a mixture of 50 eV Ar^+-N^{2+}-N^+ ions during deposition. Coatings hardness was measured using a nanoindenter equipped with a Berkovich diamond pyramid. The residual stress in the coatings was determined using XRD analysis and crystallite group method that is adapted to textured coatings and films. The results are compared to the conventional $\sin^2\psi$ method. Our results show that for the films deposited at 573K the increase in Ni content results in a decrease of coating residual stresses. For films deposited at room temperature residual stresses remain nearly constant, except around 5 at.% Ni where significant reduction is observed. For both temperatures, the hardness increases and exhibits a maximum in the range 5 to 10 at.% Ni. Our results show that the hardness enhancement in TiN-Ni nanocomposite coatings is not correlated with residual stresses, but rather to intrinsic nanostructure.

1. INTRODUCTION

Nanocomposite coatings have recently attracted increasing research interest, due to the possibility of synthesizing materials with unique physical and mechanical properties like superhardness [1,2]. They consist of two phases: one is composed of nanocrystalline transition metal nitride grains and the other is generally an amorphous intergranular phase covering the surfaces of the nitride nanocrystals [3,4]. Most PVD methods used to deposit nanocomposite coatings are based on reactive magnetron sputtering; however ion beam assisted deposition technique could be very useful for controlling independently the atomic vapour and reactive assistance with nitrogen ions [5,6]. The bombardment of a growing film with energetic ions is a very successful technique to produce very dense films. However the build up of compressive stresses occurs when the energy of atomic species is above about few tens of eV and is attributed to an “atomic peening” mechanism [7]. Excessive values of intrinsic stress are not desirable for most applications because they will result in film failure. The ion beam assisted deposition technique used in this work for the synthesis of Ti-Ni-N nanocomposite coatings results in a high level of biaxial compressive stresses in the films and an important question to address is whether hardness increase is mainly due to the nanostructure itself or to the compressive stress in the coatings. In recent years a great deal of research has been de-

Corresponding author: Jean Paul Riviere, e-mail: jean.paul.riviere@univ-poitiers.fr

voted to the synthesis of hard and superhard coatings where the hardness enhancement is not only due to the high compressive stresses [3,8-10]. In this paper, we report results on Ti-Ni-N films deposited by Reactive Dual Ion Beam Sputtering (RDIBS) to obtain a nanocomposite structured coating and compare the hardness and compressive stress evolutions.

2. EXPERIMENTAL DETAILS

~0.5 μm thick TiN films containing from 0 up to 22 at.% Ni were deposited at substrate temperatures of T_s=*RT* and 573K, using an ultrahigh vacuum NORDIKO-3000 ion beam sputtering system equipped with two RF plasma sources and two cryogenic pumps (base pressure ≤$1.33 \cdot 10^{-6}$ Pa). A Ti-Ni composite target was sputtered with 1.2 keV Ar^+ ions while the growing film is bombarded with a mixture of 50 eV Ar^+-N^{2+}-N^+ ions during deposition [11]. The angle between the secondary beam and the substrate was 45°. The N_2 and Ar flows of the assisted beam were held constant at 2 sccm for the whole set of samples. During deposition, the total pressure in the chamber was $3.33 \cdot 10^{-2}$ Pa and the target-to-substrate distance was 30 cm. Two different substrates were used: Si(100) wafers covered with native oxide (approx. 2 nm thick) for chemical and structural analysis and mirror polished (R_a~0.01-0.014 μm) 304L stainless steel disks with hardness of 240 H_v (100 g) for nanoindentation and tribological tests. All substrates were successively cleaned for 15 min in two ultrasonic baths containing acetone and ethyl alcohol respectively. Coating thickness was determined using a surface profilometer Dektak II system. The film composition was obtained from Rutherford backscattering spectroscopy (RBS) using 3.2 MeV He^{+2} ion beam at the ARAMIS facility, Orsay France. The analysis of the RBS spectra was carried out using the SIMNRA software [12]. The existing phases and crystallographic structure of the deposited films were examined using a Siemens (D5005) diffractometer operating at 40 kV and 30 mA, equipped with a secondary monochromator selecting the Cu K_α radiation. Stress analysis was performed using the crystallite group method (CGM), based on the $\sin^2\psi$ method, developed to stress evaluation in textured materials and coatings [13]; all crystallites with the same orientation are treated as being one crystal. After determining the strains for TiN (200) and TiN (111) oriented grain groups, the stress state was evaluated using linear elastic theory [14] and elastic data

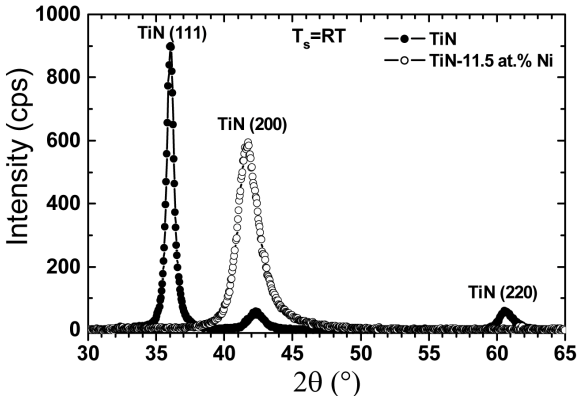

Fig. 1. θ-2θ XRD pattern of TiN and TiN-11.5 at.% Ni nanocomposite coatings deposited at T_s=RT.

of single crystalline TiN obtained from ref. [15]. Measurements were performed on a four-circle diffractometer using a Cu X-ray source with a 1´1 mm^2 point focus equipped with a Ni filter in the direct beam path to absorb the Cu K_β radiation. The incident beam was collimated using a 1 mm-diam collimator and focused on the sample mounted on an Eulerian cradle for ψ tilting, where ψ is the angle between the specimen surface and the scattering plane. Hardness tests were performed using a nano hardness tester equipped with a Berkovich diamond pyramid. The tests were performed at RT in the force-control mode of the machine. A three steps loading, holding and unloading cycle was used, every step lasting 30 sec. The calibration procedure suggested by Oliver and Pharr [16] was used to correct for the load-frame compliance of the apparatus and the imperfect shape of the indenter tip. The maximum load was varied between 0.2 mN and 300 mN, and it appeared that 1.5 mN was the optimum load according to the 10% penetration depth rule [17]. The given results are the average of 15 measurements with standard deviation used as error bars.

3. RESULTS

3.1. Microstructure

Fig. 1 shows typical θ-2θ XRD patterns of TiN and TiN-11.5 at.% Ni nanocomposite coatings deposited at T_s=RT. The XRD measurements in θ-2θ and grazing incidence configurations, for films depos-

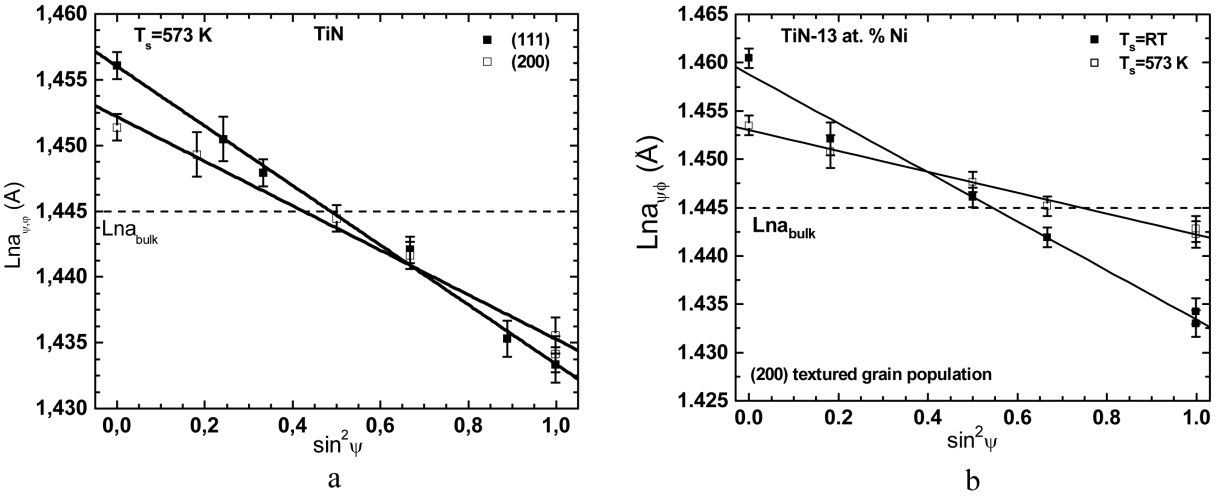

Fig. 2. $\sin^2\psi$ plots for (a) (111) and (200) oriented grains in TiN film deposited at T_s=573K and (b) (200) oriented grains in two TiN-13 at.% Ni nanocomposite coatings deposited at RT and 573K respectively.

ited at T_s=RT and 573K, indicates the presence of TiN peaks and no reflections from neither Ni nor Ni containing compounds indicating that Ni appears as an amorphous phase, even up to 22.5 at.% Ni. Texture evolution takes place from TiN (111) to TiN (200) with Ni content and beyond 10 at.% Ni a pure (200) texture develops. Addition of Ni causes a monotonous decrease in grain size from about 12nm for single phase polycrystalline TiN to about 4nm for TiN-22 at.% Ni nanocomposite coating. The similar evolutions in existing phases, coating texture and grain size were previously observed for films deposited at 673K [6].

3.2. Residual stress

The true strain for a given {*hkl*} reflection in φ and ψ directions, is defined as:

$$\varepsilon_{\psi,\varphi}^{hkl} = \ln\frac{a_{\psi,\varphi}^{hkl}}{a_0}, \qquad (1)$$

where $a_{\psi,\varphi}$ and a_0 are the lattice parameter deduced from $d_{\psi,\varphi}\, a_{\psi,\varphi}^{hkl} = d_{hkl}\sqrt{h^2+k^2+l^2}$ corresponding to the lattice plane spacing of the {*hkl*} planes in a given ψ,φ direction and unstrained lattice parameter, respectively. Linear elasticity leads to the relation between strain and stress, $\varepsilon_{ij} = s_{ij}\sigma_{ij}$, where s_{ij} are the material elastic compliances. The general stress-strain relations using the CGM are developed for three dimensional stress conditions. In the case of thin films the stress field can be modeled to be biaxial. The simplification of related equations given by Clemens *et al.* [14] for (111) and (200) textures of fcc crystal leads to the following equations for the case of biaxial stresses:

$$Lna_{\psi,\varphi} = \left(2S_{12} + \frac{2}{3}J + \frac{S_{44}}{2}\sin^2\psi\right)\sigma + Lna_0 \qquad (2)$$

(111) fiber texture,

$$Lna_{\psi,\varphi} = \left[2S_{12} + (S_{11} - S_{12})\sin^2\psi\right]\sigma + Lna_0 \qquad (3)$$

(200) fiber texture,

where $J = S_{11} - S_{12} - S_{44}/2$ is the anisotropy factor of the material. Plotting of $Lna_{\psi,\varphi}$ against $\sin^2\psi$ yields a straight line whose slope is proportional to the residual stress amplitude and the intercept corresponds to the stress-free lattice parameter a_0. Fig. 2a compares the $\sin^2\psi$ plots respectively for (111) and (200) oriented grains in TiN film deposited at T_s=573K. The (111) oriented grain population exhibits a higher slope than that of (200) one, as revealed in Fig. 2a for pure TiN, as well as for coatings with ~5 at.% Ni (not shown). Comparing data of Fig. 2b for (200) oriented grains in two TiN-13 at.% Ni nanocomposite coatings, reveals that coating deposited at T_s=573K, has a lower stress level than that deposited at T_s=RT, as evidenced by a

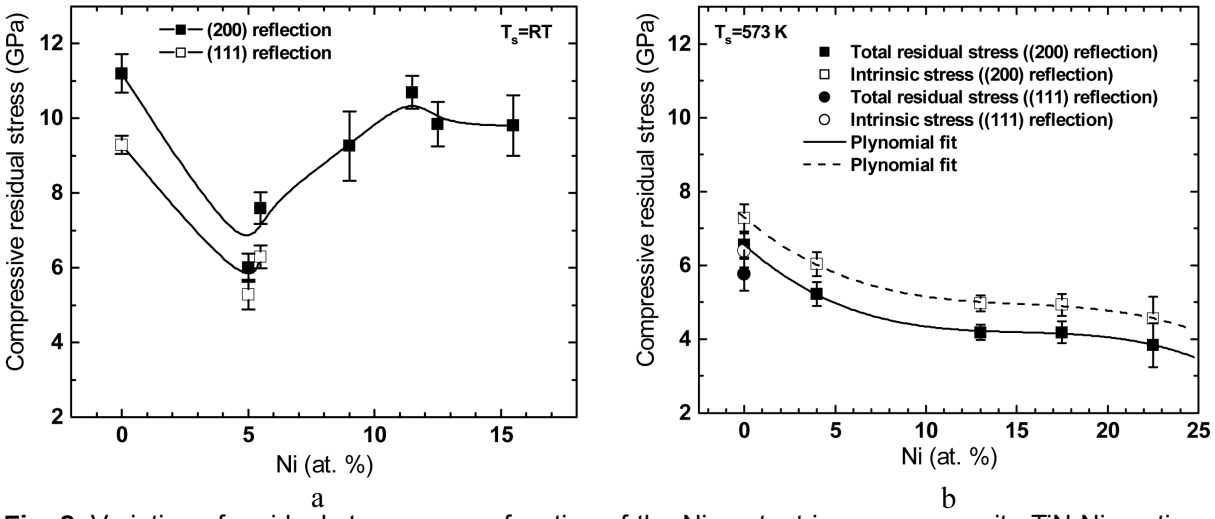

Fig. 3. Variation of residual stresses as a function of the Ni content in nanocomposite TiN-Ni coatings deposited at (a) T_s=RT and (b) T_s=573K.

significant decrease in the slope of the $\sin^2\psi$ lines. Fig. 3 shows the variation of total residual stress (TRS) as a function of Ni concentration at substrate temperatures of RT and 573K, respectively. These values were calculated from the slope of $\sin^2\psi$ plots similar to the plots shown in Fig. 2 and using single crystal TiN elastic constants obtained from ref. [15]. These values give a Young modulus value for single crystal TiN which is closer to what has been measured for polycrystalline TiN coatings studied in this work. The single crystal TiN elastic constants leads to Young's modulus values of 451 GPa, 417 GPa, and 424 GPa for (111), (200), and (220) directions, respectively, while values of 336 GPa and 316 GPa were measured for understiochiometric polycrystalline TiN deposited at RT and 573K, respectively. The use of the CGM itself (misoriented grains are not taken into account) and the above mentioned elastic constants results to overestimation of stress values. However, for the purpose of studying the stress evolution with Ni content the present analysis is valuable.

At T_s=573 K the intrinsic stresses, calculated after removing the thermal stress contribution, are also presented in Fig. 3b. For coatings deposited at RT higher stress amplitudes were obtained than at 573K. For both temperatures the addition of a little amount of Ni reduces the stress, as compared to that of single crystal TiN that is very strong at RT. For coatings deposited at T_s=573K a monotonous stress decrease is observed from 6.6 GPa for TiN to 3.8 GPa for TiN-22.5 at.% Ni coatings. A distinct behavior is found for coatings deposited at RT: stress decreases from 11.2 GPa for TiN to a minimum of 6.6 GPa at about 5 at.% Ni, it increases again reaching to about 10 GPa and remains constant up to 15.5 at.% Ni. The stress analysis using classical $\sin^2\psi$ method, i.e. plotting of $\sin^2\psi$ plots at different ψ angles applied to a given reflection (in this work the (111), (200) and (220) reflections were used separately) for selected samples and using experimentally measured elastic constants (via nanoindentation), resulted in a similar trend for the stress evolution with Ni content. However calculated stresses values are lower than those obtained from the CGM. The main drawback using classical $\sin^2\psi$ method was the limited data points in $\sin^2\psi$ plots because of the textured nature of films which makes difficult its application for high Ni content films with pure (200) texture.

3.3. Hardness

Fig. 4 represents the variations of the nanocomposite coatings hardness as a function of the Ni content in comparison with pure TiN (0 Ni at.%) for coatings synthesized at T_s=RT and 573K. It is seen that the hardness of nanocomposite coatings increases with Ni addition for both temperatures. At T_s=RT a maximum hardness of 44.2 ±

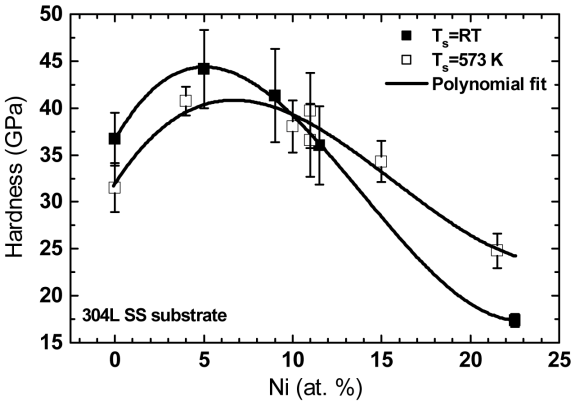

Fig. 4. Variations in the hardness of nanocomposite TiN-Ni coatings as a function of the Ni content for coatings synthesized at T_s=RT and 573K.

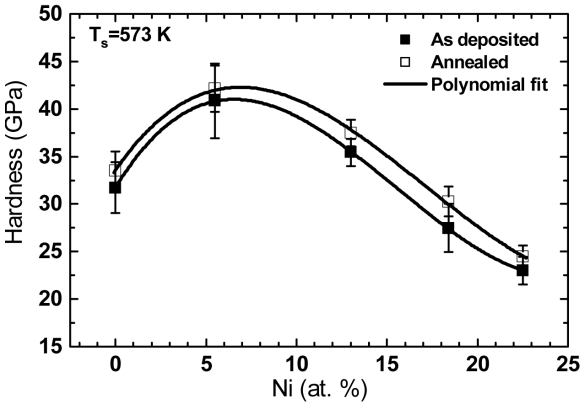

Fig. 5. Hardness of nanocomposite TiN-Ni coatings as a function of Ni content before and after annealing for 1 hour at 773K on M2 tool steel substrate.

4.2 GPa is reached at about 5 at.% Ni, corresponding to a hardness enhancement of about 20% with respect to the single phase TiN deposited under the same conditions. Coatings hardness remains higher than 40 GPa up to 10 at.% Ni, and finally decreases down 17.4 ± 0.7 GPa for Ni content of 22.5 at.% Ni. At T_s=573K a similar evolution in hardness vs. Ni content is observed. However, lower hardness values were obtained for TiN and nanocomposite coatings up to 10 at.% Ni, with a maximum hardness of about 41 GPa corresponding to about 30% increase with respect to the related pure TiN. Beyond 10 at.% Ni the hardness decreases more slowly than at T_s=RT, leading to a larger Ni content range with enhanced hardness. At 22.5 at.% Ni about 7 GPa higher hardness value was obtained for coating deposited at T_s=573K than at T_s=RT.

3.4. Thermal stability

Fig. 5 depicts the nanocomposite coatings hardness as a function of the Ni content before and after annealing under vacuum (~10^{-4} Pa) for 1 hour at 773K. The hardness values after heat treatment indicate a ~1-2 GPa increase depending on Ni content with respect to the as deposited coatings. Even if the values are in the uncertainty intervals of measurements and can not be taken into account, they clearly indicate the thermal stability of the coatings hardness under the studied heating conditions.

4. DISCUSSION

The development of nanocomposite structure is the result of the segregation of Ni atoms during film growth which interrupts the growth of TiN crystallites and forces the renucleation of new crystallites. Like the segregation of active impurities [18], the segregation of Ni takes place by the atom-by-atom building process and the subsequent formation of a tissue of solid phase Ni around the TiN crystallites. Such mechanism not only explains the observed reduced size of TiN grains, but also that they are embedded in an amorphous matrix of Ni with thickness of 1-2 monolayers. At T_s=573K the thermal residual stresses (TRS) and intrinsic stresses decrease monotonically with the Ni content and the maximum stress is obtained for TiN films, while the hardness as a function of the Ni content increases and reaches a maximum at a Ni content between 5 to 10 at.% Ni. Then hardness decreases with further Ni addition. The maximum in hardness corresponds to about one monolayer of Ni coverage [6]. The reduction in stress with Ni content is related to the repeated nucleation of TiN crystallites caused by the Ni segregation in the development of nanocomposite structure resulting in grain size reduction and texture change provid-

ing possibility to self arranging mechanism to reduce internal energy. The reduction in stress with Ni composition implies that the hardness enhancement is due to the development of a nanocomposite structure rather than to the effects of residual stresses. At T_s=RT the residual stress first decreases until 5 at.% Ni then increases with further increase in Ni content but the variation in hardness does not follow the variation of residual stress and exhibits the similar variation as for coatings deposited at T_s=573K. Comparison of the variation in residual stress (Fig. 3a) and hardness (Fig. 4) indicates that their evolutions with Ni content is opposite from 0 to about 10 at.% Ni and the maximum hardness corresponds to the minimum in residual stress. The nanocomposite coatings containing more than 10 at.% Ni content, at T_s=RT, exhibit more rapid decrease in hardness with increasing Ni, than coatings deposited at T_s=573K while the variation of residual stresses within this range of composition is just the opposite; stress values are twice higher at RT than 573K. Therefore, at T_s=RT also the variation of hardness does not follow the variation of residual stresses; indicating that hardness enhancement is due to the formation of a nanocomposite structure. The higher values of stresses obtained at RT can be explained in terms of a higher defect density in TiN and nanocomposite coatings. For TiN coatings increasing substrate temperature resulted in lower residual stresses, which can be attributed to the higher adatom mobilities causing the defects annihilation [19,20]. For nanocomposite coatings, more effective adatom mobility is needed not only for defect density reduction in TiN crystallites but also for effective Ni segregation and formation of separate crystalline TiN and amorphous Ni phases. For lower mobility, such as RT, the TiN crystallites and Ni/TiN phase boundaries will be more disordered resulting in a microstructure far from thermodynamic equilibrium than coatings deposited at higher temperatures. This effect can be important with increasing Ni content. Moreover, other source of increased hardness is the probable incorporation of a little amount of Ni atoms (less than 1 at.%) in TiN lattice, for example in N sites. Recent calculations for single phase TiN shows that misfit Ti atoms (less than 1 at.%) in N sites may lead stresses of several GPa [21]. The more rapid decrease in hardness for coatings deposited at RT than for those at 573K could be explained by a more defective structure of these coatings, as plastic deformation takes place via grain boundaries. In TiN-Ni nanocomposite coatings the thermal stability is more or less governed by the thermomechanical properties of the soft metallic matrix, rather than those of the TiN crystallites, while in nc-TiN/a-ceramic coatings both phases are equally important. However, in optimized nanocomposite structure the thickness of amorphous Ni phase embedding TiN crystallites remains less than two monolayers, even up to 22.5 at.% Ni in the coatings studied here. Except at very high annealing temperatures, the thin Ni layer withstands to precipitate as large crystalline or amorphous grains. This amorphous tissue inhibits TiN grain growth and coalescence during annealing and therefore enhancing structure and hardness stabilities.

5. CONCLUSIONS

The TiN-Ni nanocomposite coatings deposited using RDIBS show enhanced hardness up to 15 at.% Ni depending on substrate temperature. The hardness enhancement was observed to be due to the nanocomposite structure. No correlations were found between hardness enhancement and residual stresses. The nanocomposite coatings exhibit thermal stability up to 773K.

ACKNOWLEGEMENTS

The authors gratefully acknowledge the CSNSM (Orsay) for RBS analysis performed with the ARAMIS facility. A. Akbari thanks MSRT of Iran for financial support during his PhD work.

REFERENCES

[1] S. Vepřek, A. Niederhofer, K. Moto, T.Bolom, H.D.Mannling, P. Nesladek, G. Dollinger and A. Bergmaier // *Surf. Coat. Technol.* **133-134** (2000) 152.

[2] F. Vaz, L. Rebouta, P. Goudeau, J. Pacaud, H. Garem, J. P. Rivière, A. Cavaleiro and E. Alves // *Surf. Coat. Technol.* **133-134** (2000) 307.

[3] A. Niederhofer, T. Bolom, P. Nesladek, K. Moto, C. Eggs, D.S. Patil and S. Vepřek // *Surf. Coat. Technol.* **146-147** (2001) 183.

[4] S. Zhang, D. Sun, Y. Fu and H. Du // *Surf. Coat. Technol.* **167** (2003) 113.

[5] J.S. Colligon, V. Vishnyakov, R. Valizadeh, S.E. Donnelly and S. Kumashiro // *Thin Solid Films* **485** (2005) 148.

[6] A. Akbari, J.P. Riviere, C. Templier and E.Le Bourhis // *Surf. Coat. Technol.* **200** (2006) 6298.
[7] H. Windishmann // *Crit. Rev. Sol. St. Mat. Sci.* **17** (1992) 547.
[8] J. Musil, H. Hruby, P. Zeman, H. Zeman, R. Cerstvy, P.H. Mayflrhofer and C. Mitterer // *Surf. Coat. Technol.* **142-144** (2001) 603.
[9] S. Vepřek // *J.Vac.Sci.Technol.* **A17** (1999) 2401.
[10]. E. Ribeiro, L. Rebouta, S. Carvalho, F. Vaz, G.G. Fuentes, R. Rodriguez, M. Zazpe, E. Alves, Ph. Goudeau and J.P. Riviere // *Surf. Coat. Technol.* **188-189** (2004) 351.
[11] G. Abadias and Y. Y. Tse // *Surf. Coat. Technol.* **180 –181** (2004) 33.
[12] M. Mayer, In: *Proceedings of the 15th International Conference Applications of Accelerators in Research and Industry*, ed. by J.L.Duggan and L.L.Morgan // *AIP Conf.Proc.* **475** (1999) 541.
[13] V. Hauk, *Structural and Residual Stress Analysis by Nondestructive Methods* (Elsevier, Amsterdam, 1997).
[14] B.M. Clemens and J.A. Bain // *MRS bulletin* **17** (1992) 46.
[15] M. Zhang and J. He // *Surf. Coat. Technol.* **142-144** (2001) 125.
[16] W. C. Oliver and G. M. Pharr // *J. Mater. Res.* **7** (1992) 1564.
[17] A. K. Bhattacharya and W.D. Nix // *Int. J. Solids Struct.* **24** (1986) 1287.
[18] P.B. Barna , M. Adamik , J. Lábár , L. Kövér , J. Tóth , A. Dévényi and R. Manaila // *Surface and Coatings Technology* **125** (2000) 147.
[19] H. Ljungcrantz, L. Hultman and J.-E. Sundgren // *J. Appl. Phys.* **78** (1995) 832.
[20] G. Abadias, Y. Y. Tse, and Ph. Guérin and V. Pelosin // *J. Appl. Phys.* **99** (2006) 113519.
[21] J.-D. Kamminga, Th. H. de Keijser and R. Delhez // *J. Appl. Phys.* **88** (2000) 6332.